JGR Oceans

RESEARCH ARTICLE
10.1029/2020JC016377

Transport and Evolution of the East Reykjanes Ridge Current

G. Koman[1], W. E. Johns[1], and A. Houk[1]

[1]Rosenstiel School of Marine and Atmospheric Science, University of Miami, Miami, FL, USA

Key Points:
- The East Reykjanes Ridge Current forms from a convergence of the North Atlantic Current and deeper Icelandic Slope Water south of Iceland
- The East Reykjanes Ridge Current flows along the Reykjanes Ridge at 10–13 Sv before retroflecting into the Irminger Current near 59°N
- The East Reykjanes Ridge Current is responsible for about one third of the net potential density change around the rim of the subpolar gyre

Correspondence to:
G. Koman,
gkoman@rsmas.miami.edu

Citation:
Koman, G., Johns, W. E., & Houk, A. (2020). Transport and evolution of the East Reykjanes Ridge Current. *Journal of Geophysical Research: Oceans*, *125*, e2020JC016377. https://doi.org/10.1029/2020JC016377

Received 5 MAY 2020
Accepted 24 SEP 2020
Accepted article online 25 SEP 2020

Abstract This study of the first continuous multiyear observations of the East Reykjanes Ridge Current (ERRC) reveals a highly variable, mostly barotropic southwestward flow with a mean transport of 10–13 Sv. The ERRC effectively acts as a western boundary current in the Iceland Basin on the eastern flank of the Reykjanes Ridge. As part of the Overturning in the Subpolar North Atlantic Program (OSNAP), continuous measurements of the ERRC have been maintained for the first time using acoustic Doppler current profilers, current meters, and dynamic height moorings at six mooring sites near 58°N since 2014. Together with satellite altimetry and Argo profile and drift data, the mean transport, synoptic variability, water mass properties, and upstream and downstream pathways of the ERRC are examined. Results show that the ERRC forms in the northeastern Iceland Basin at the convergence of surface waters from the North Atlantic Current and deeper Icelandic Slope Water formed along the Iceland-Faroe Ridge. The ERRC becomes denser as it cools and freshens along the northern and western topography of the Basin before retroflecting over the Reykjanes Ridge near 59°N into the Irminger Current. Analysis of the flow-weighted density changes along the ERRC's path reveals that it is responsible for about one third of the net potential density change of waters circulating around the rim of the subpolar gyre.

Plain Language Summary The East Reykjanes Ridge Current (ERRC) is an important but poorly studied flow in the Iceland Basin of the northern North Atlantic Ocean. This study investigates the ERRC using underwater floats, satellites, and 4 years of continuous mooring data to determine the current's pathways, water properties, and the strength of its transport. From its formation to the south of Iceland near 62°N, 18°W, the ERRC travels westward along the Icelandic slope before turning to the southwest as it follows the eastern flank of a shallow portion of the Mid-Atlantic Ridge, known as the Reykjanes Ridge. As the Reykjanes Ridge deepens, the ERRC eventually reaches its termination as it crosses westward over the ridge into the next basin. Results of this study show that the ERRC is approximately 900 km in length and has an average transport of 10–13 Sv (1 Sv = 1,000,000 m^3/s). Significant water densification occurs along the ERRC's path, which makes it an important component in the broader picture of the Earth's climate system.

1. Introduction

Knowledge of the circulation of the North Atlantic subpolar gyre is fundamental to a deeper understanding of the global meridional overturning circulation. The subpolar gyre has experienced large changes over recent decades, including a pronounced freshening since 2015 (Holliday et al., 2020) and is one of the few locations on the planet that is actually cooling in response to Climate Change (Hermanson et al., 2014). The Atlantic Meridional Overturning Circulation (AMOC) in the subpolar North Atlantic is intimately linked to the horizontal circulation of the subpolar gyre due to the progressive modification of upper ocean waters as they circulate cyclonically around the gyre and lose buoyancy. Understanding how and where these waters are modified as they circulate around the gyre, and the pathways and transports of the main current systems that carry them, will give a better insight into the densification process of the overturning. In this paper we focus on the East Reykjanes Ridge Current (ERRC)—an important but poorly studied component of the Iceland Basin circulation—using observations from OSNAP to quantify its transport and variability, and additional observations from Argo and altimetry to understand its sources and evolution through the basin.

The East Reykjanes Ridge Current forms in the northern Iceland Basin where a portion of the warm, salty waters of the North Atlantic Current turn westward at the Iceland-Faroe Ridge to flow adjacent to the southern Icelandic slope before turning southwestward along the eastern flank of the Reykjanes Ridge (Figure 1).

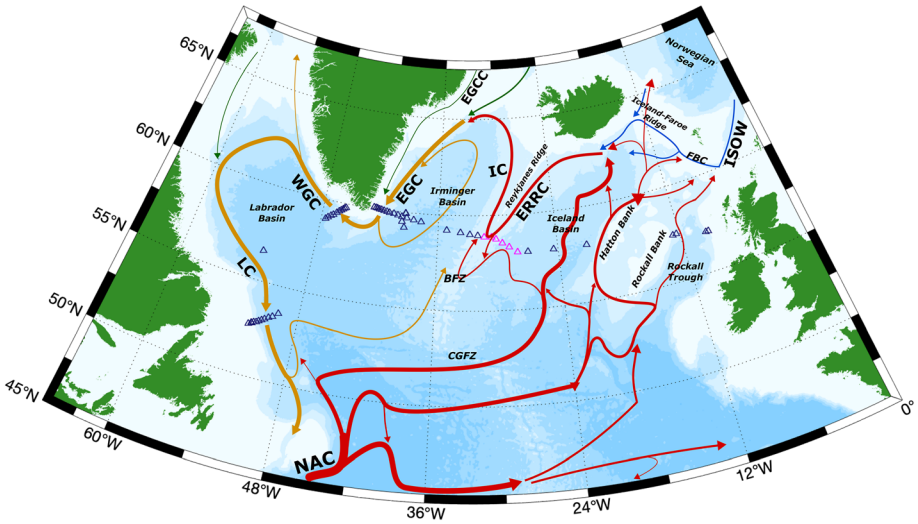

Figure 1. Schematic of the surface water pathways (red, yellow, and green) and deep water pathways (blue) relevant to this study in the North Atlantic subpolar gyre, adapted from Daniault et al. (2016) and refined by the results of this study. Green and red arrows depict surface waters primarily of Arctic origin and North Atlantic Current origin, while yellow arrows represent surface waters with mixtures of both. All mooring locations in the OSNAP program are denoted by triangles with the moorings used in this study in magenta. Bathymetry colors change with every 1,000 m in depth. Acronyms: East Reykjanes Ridge Current (ERRC); Irminger Current (IC); East Greenland Coastal Current (EGCC); East Greenland Currents (EGC); West Greenland Current (WGC); Labrador Current (LC); North Atlantic Current (NAC); Iceland Scotland Overflow Water (ISOW); Faroe Bank Channel (FBC); Charlie Gibbs Fracture Zone (CGFZ); Bight Fracture Zone (BFZ).

Through deep winter convection, this water transforms into Subpolar Mode Water (Brambilla & Talley, 2008) and constitutes the surface waters of the ERRC. The remainder of the North Atlantic Current flow that does not circulate cyclonically in the Iceland Basin crosses the Iceland-Faroe Ridge to provide source waters for deep convection in the Norwegian Sea. While the existence of the ERRC has been recognized for decades, it has only been quantitatively studied since about 2000 through hydrographic surveys (Daniault et al., 2016; Mercier et al., 2015; Sarafanov et al., 2012) and repeated shipboard Acoustic Doppler Current Profiler (ADCP) sections (Chafik et al., 2014; Knutsen et al., 2005). The ERRC was not even named until 2005 (Treguier et al., 2005), as most previous studies in the area had focused on Iceland Scotland Overflow Water instead of the upper water column (Kanzow & Zenk, 2014; Van Aken & De Boer, 1995). Repeated ADCP sections from a container vessel, the Nuka Arctica, between Greenland and Denmark in the early 2000s show a 0.1-m s^{-1} flow in the upper 200 m of the ERRC (Chafik et al., 2014; Knutsen et al., 2005), while drifter data in the region have shown a slower surface flow of 0.05 m s^{-1} (van Aken & Becker, 1996). A recent synoptic study from the summer of 2015 (Petit et al., 2019) gives the ERRC transport estimates of 13.8 Sv near 62°N and 10.6 Sv near 58°N, while repeat full water hydrographic sections from the Observatory of Interannual and Decadal Variability in the North Atlantic project (OVIDE) have revealed a southwestward transport of ~9 Sv that could be classified as ERRC waters (σ_θ < 27.8 kg m^{-3}) (Daniault et al., 2016). The OVIDE analysis also suggests that there may be two branches of the ERRC: a western portion that extends barotropically through the water column connecting with Iceland Scotland Overflow Water at the bottom and an eastern part that has a much shallower flow. Shipboard ADCP data suggest that the ERRC reaches a peak velocity in autumn (Knutsen et al., 2005), but the seasonality of the current is not well understood. Given these scarce observations of the ERRC, establishing a comprehensive record of the current through time series observations is of utmost importance.

In this study we derive transport estimates of the ERRC from 4 years of continuous observations as part of the Overturning in the Subpolar North Atlantic Program (OSNAP). Starting in 2014, OSNAP has maintained the first continuous Eulerian array across the entire North Atlantic subpolar gyre to improve our knowledge of the gyre's transbasin fluxes of heat, mass, and freshwater. In the Iceland basin, six OSNAP moorings are situated on the western side of the basin and over the Reykjanes Ridge near 58°N to monitor the transport

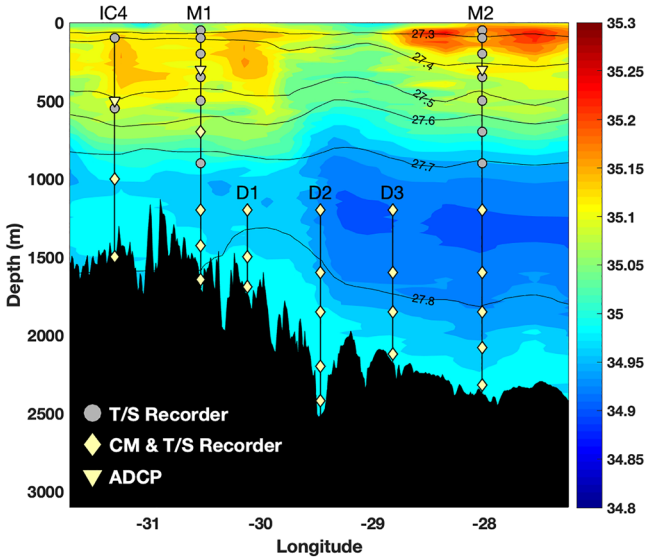

Figure 2. Southern view of the OSNAP moorings used in this study down the eastern flank of the Reykjanes Ridge near 58°N. Colored contours show salinity (psu) from a section of CTD stations from the summer of 2016; black contour lines are sigma-theta surfaces (kg m^{-3}).

and variability of the ERRC. In addition to OSNAP mooring results, altimetry and Argo float data are incorporated in the analysis to examine the upstream and downstream pathways of the ERRC and to create a more robust multidecadal analysis. This study will therefore establish a comprehensive foundation on the ERRC to better inform future research in the region.

2. Data and Methods

2.1. OSNAP Moorings

The OSNAP array extends from Canada across the Labrador Basin to Greenland, and from Greenland across the Irminger and Iceland basins to Scotland (Figure 1). The array in the western Iceland Basin is arranged to capture two distinct components of the circulation: the southwestward flowing ERRC and the southwestward Iceland Scotland Overflow Water plume flowing near the bottom along the eastern flank of the Reykjanes Ridge (Figure 2). Temperature and salinity (T/S) recorders, current meters, and ADCPs have provided continuous data in three separate deployments for the period from July 2014 to July 2018. The United States-supported (University of Miami) array in this area consists of dynamic height moorings M1 and M2 to capture the majority of the ERRC as well as additional deep moorings (D1–D3) focused within the Iceland Scotland Overflow Water layer. An additional mooring maintained by the Royal Netherlands Institute of Sea Research, IC4, is also used to calculate portions of the ERRC that extend west of M1.

To derive estimates of the ERRC's transport and vertical structure, the OSNAP data are initially passed through a 40-hr low-pass filter to remove subinertial variability associated with internal/inertial waves and tides. Shape-preserving splines are then used to interpolate between T/S recorders to give full-depth property profiles at moorings M1 and M2 to within 50 m of the surface (the top measurement level on M1 and M2). To extend these profiles to the surface, the 50-m temperature readings are compared to (1/20)° satellite-derived operational sea surface temperature (OSTIA) data from the Group for High Resolution Sea Surface Temperature (GHRSST). This data are interpolated to the location of the mooring site and is produced by the Jet Propulsion Laboratory and obtained through the Asia-Pacific Data Research Center. If GHRSST is warmer than the 50-m temperature, GHRSST is used as the surface temperature point in the vertical spline interpolation; otherwise, the 50-m temperatures are extended to the surface. The latter scenario only occurs when a deep mixed layer is present but yields much more accurate results based on an analysis comparing Argo surface temperatures to 50-m Argo temperatures and GHRSST. Lacking any more accurate estimate of surface salinity, measured salinity values at 50 m were duplicated to the surface. Using these full-depth T/S profiles, the horizontally averaged geostrophic velocity profile is calculated between moorings M1 and M2 and expressed as a transport-per-unit-depth profile between the two moorings. These profiles are then integrated with depth to 1,200 m to give the baroclinic geostrophic transport relative to that depth and referenced to the horizontally averaged velocity measured by the five current meters deployed at 1,200-m depth on moorings M1, D1, D2, D3, and M2. This provides an absolute estimate of the transport-per-unit-depth profile and total transport between moorings M1 and M2. To obtain the transport deeper than 1,200 m, current meter data from these five moorings is gridded and integrated for all waters above the $\sigma_\theta = 27.8$ kg m^{-3} isopycnal. Transport below 27.8 kg m^{-3} is considered to be part of the Iceland Scotland Overflow Water plume (Dickson & Brown, 1994; Saunders, 1996) and is not included in our derived transport estimates for the ERRC.

Between M1 and the Dutch-maintained IC4 to the west, current meter and ADCP readings from the two moorings are interpolated over the Reykjanes Ridge to determine the time-varying zero-velocity boundary between the southward flowing ERRC and the northward flowing Irminger Current. The southward flowing waters east of this zero-velocity line are integrated and summed with the previously described estimates between M1 and M2 to determine the total transport of the ERRC near 58°N.

2.2. Aviso+ and CMEMS All-Satellite Altimetry

The Aviso+ absolute sea level product comes from multimission altimeter satellites and is processed to a (¼)° gridded sea surface height computed with respect to its 20-year mean since 1992. Prior to 2016, these data were offered through AVISO+ but since then the European based Copernicus Marine Environmental Monitoring Service (CMEMS) has been responsible for its distribution. The absolute dynamic topography derived from this product is used to calculate surface reference velocities between moorings M1 and M2 to produce an alternate estimate of the absolute geostrophic transport between those two moorings (i.e., using the altimeter-derived surface reference velocities instead of the 1,200-m current meter reference velocities). This daily product is interpolated to hourly data as an integrated transport-per-unit-depth at the sea surface ($m^2\ s^{-1}$), which is then added to the baroclinic geostrophic transport profile between M1 and M2. Vertical integration of this profile then leads to an altimetry-referenced estimate of absolute transport between M1 and M2.

This study also uses mean surface velocities derived from the (¼)° altimeter product from 1992 until 2018 to help determine the evolution of the ERRC through the basin as well as the broader structure of surface currents in the Iceland Basin. These data are combined with (¼)° interpolated Argo data to calculate transport values along the ERRC's path including its eventual termination over the Reykjanes Ridge.

2.3. Argo Data

Argo profile data are taken from the Roemmich-Gilson Argo climatology, which is created and distributed by the Scripps Oceanographic Institution. This product contains temperature and salinity data at 58 different pressure levels and has global coverage of (⅙)° resolution for the mean field and (½)° resolution for the annual cycle (Roemmich & Gilson, 2009). The (⅙)° mean product, based on data from 2004–2016, is used to determine the baroclinic component of transport in the water column and mean water mass properties of the ERRC.

Argo displacement drift data, which is used to calculate velocities at the 1,000 m parking level based on the displacement of Argo floats between diving cycles (Lebedev et al., 2007), is used as a reference velocity to help determine the upstream and downstream pathways of the ERRC. This (¼)° mean product includes data from 1997 to 2016 and is made available through the Asia-Pacific Data Research Center (APDRC). The Argo-derived baroclinic shear is interpolated to (¼)° and referenced to the 1,000-m Argo drift displacement data to resolve Argo-based mean velocities throughout the upper 2,000-m water column (Bilo, 2019; Bilo & Johns, 2019). These data are also used in transport calculations along a number of sections across the ERRC (e.g., Figure 8) by integrating all velocities shallower than $\sigma_\theta = 27.8$ kg m^{-3} that are within the domain and direction of the ERRC (see Figure 9). The Argo-derived shear is also referenced to surface altimetry to calculate velocities near the crest of the Reykjanes Ridge where insufficient subsurface Argo drift data is available. Finally, the (½)° Argo product is used to describe seasonal water mass changes in the ERRC.

2.4. Shipboard Hydrographic and ADCP Data

CTD casts with lowered ADCP (LADCP) and shipboard ADCP (SADCP) have been conducted on each OSNAP mooring deployment cruise (during the summers of 2014, 2015, 2016, and 2018). Within the Iceland Basin, these casts were performed ~30 km apart while the casts near topographic features—including the Reykjanes Ridge—were more closely spaced (~10–15 km). These data are used to determine synoptic transport estimates of the ERRC to compare with the mooring-based ERRC transport calculations.

On cruises where high-quality vessel mounted ADCP data was available, the mean velocity between CTD stations from 75 kHz SADCP data was combined with baroclinic geostrophic velocities determined by temperature and salinity data from CTDs to calculate transports. The LADCP data were independently gridded and integrated across each section to estimate transports. In 2018, an additional transport estimate exclusively from gridding and integrating 38-kHz SADCP data was also calculated. In 2015, only LADCP data were available. Data from 2016 are not included in this analysis due to a medi-vac emergency that resulted in the shipboard ERRC hydrographic measurements being highly asynoptic.

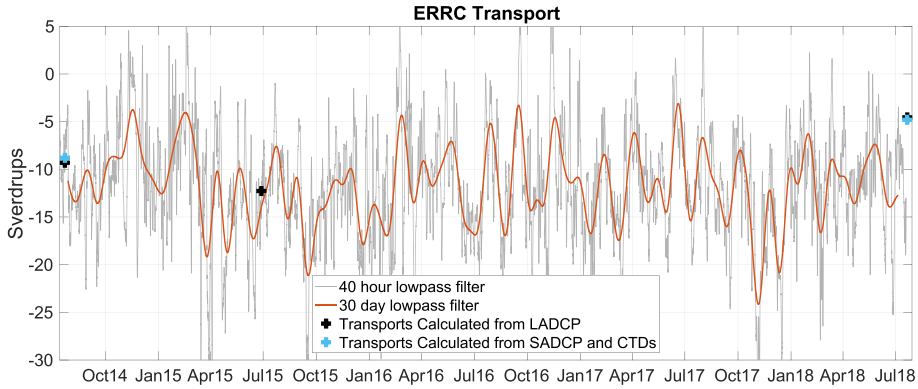

Figure 3. Transport time series of the East Reykjanes Ridge Current from 4 years of OSNAP data. Negative values are in the prevailing direction of the ERRC to the southwest. The gray curve is the transport with a 40-hr low-pass filter applied and the red curve is the transport with a 30-day low-pass filter. This total transport ($\sigma_\theta < 27.8$ kg m^{-3}) uses current meters to calculate the transport below 1,200 m, current meters and ADCPs to calculate the transport between moorings IC4 and M1, and dynamic height moorings referenced to current meters to calculate the transport between moorings M1 and M2 above 1,200 m. The ERRC has a mean southwestward transport of −11.7 Sv, with a standard deviation of 6.0 Sv and a standard error of 0.5 Sv. Crosses indicate synoptic transport estimates using LADCP (black) and combined SADCP with geostrophic shear (aqua) from cruises.

3. Results

3.1. OSNAP Array

The 4 years of transport estimates of the East Reykjanes Ridge Current derived from the OSNAP mooring data reveal a flow of significant temporal variability and a mean southwestward transport of 11.7 Sv (Figure 3). The standard error of the transport time series is 0.5 Sv, based on a calculated integral time scale of only 5.3 days (Emery & Thomson, 2001). This short decorrelation time scale gives the time series a robust 139 degrees of freedom, which yields a relatively low standard error despite a relatively high standard deviation (6.0 Sv).

In the 30-day low-pass-filtered transport time series, the ERRC transport ranges from about 5 to 20 Sv without any detectable seasonal variation. The 40-hr low-pass filtered data show much greater temporal variations from over 35 Sv in the predominant southwestward direction to more than 10 Sv in the reverse direction to the northeast. These occasional transport reversals have a very short duration, on the order of days, and are linked to significant eddy activity in the area and surges in northward transport near mooring M2.

When available, shipboard data are used to calculate the transport of the ERRC for comparison. This is done using two methods: from gridded LADCP data, and from dynamic height calculations using CTD casts referenced to upper ocean SADCP data collected along the CTD section (Figure 3). In 2014, immediately after the initial mooring deployment, the current meter-derived transport (10.1 Sv) compares well with the LADCP (9.3 Sv) and the SADCP-referenced geostrophic transport (8.8 Sv). In 2015 the data also show good agreement between the current meter-derived transport (13.5 Sv) and the LADCP estimate (12.3 Sv). In 2018, the time series estimate (12.4 Sv) was more than double the LADCP (4.6 Sv) and SADCP-referenced geostrophic (4.8 Sv) estimates, but these results are not simultaneous as the synoptic data was collected more than 2 days later than the final time series transport value. Analysis of our ERRC transport time series shows that there is a one in seven chance of this type of transport change in a 48-hr period; therefore, much of this discrepancy could be explained by the high temporal variability of the current and this comparison will need to be updated after the next recovery.

Figure 4 displays Hovmoller plots between moorings IC4 and M2 of surface geostrophic velocities inferred from altimetry and 1,200-m velocities derived from current meters. The images include velocities over the Reykjanes Ridge in the west and well into the Iceland Basin to the east in order to encompass the full breadth of the ERRC. Both figures show that the ERRC is a relatively narrow flow of ~80 km isolated to the eastern flank of the Reykjanes Ridge between moorings M1 and D2, though the altimetry suggests the surface current is more intermittent than the 1,200-m currents, which show the ERRC as a nearly constant feature with

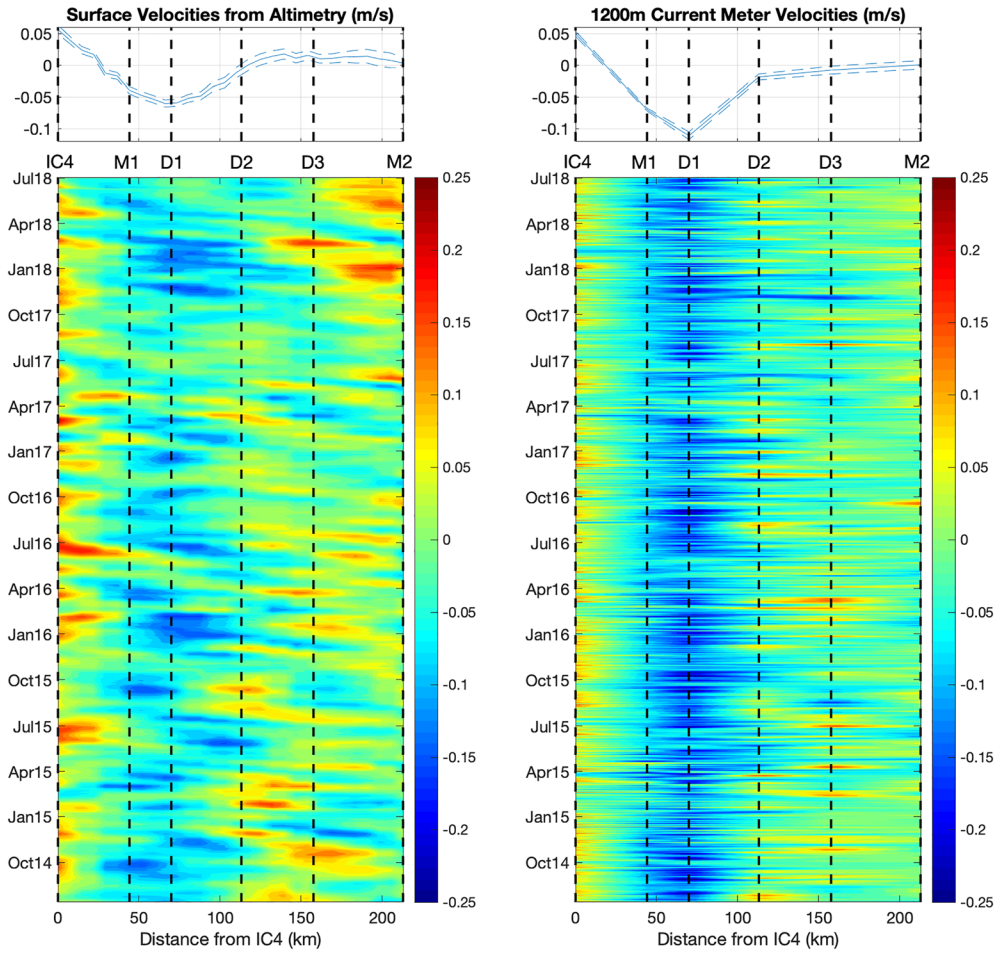

Figure 4. Hovmoller diagrams (bottom) of surface velocities (m s^{-1}) from altimetry (left) and 1,200-m velocities from current meters (right) between OSNAP moorings IC4 and M2 over a 4-year period (July 2014 to July 2018), with mooring locations denoted by black dashed lines. Negative values are in the prevailing direction of the ERRC to the southwest and distances are referenced to IC4, which is the Dutch-maintained OSNAP mooring on the western flank of ridge crest. Four-year mean velocities (top) are indicated with standard errors.

velocities greater than 0.1 m s^{-1}. Since the baroclinic component of the transport can only be calculated between dynamic height moorings M1 and M2, we evaluated the barotropic component over the same domain between M1 and M2, which includes the variability to the east of D2 where the mean flow is weak and substantial eddy signals are present.

Visual inspection of the altimetry-derived surface velocities (Figure 4, left) show the preferential westward movement of anomalies passing through the OSNAP array. Animations of the absolute dynamic topography (ADT) field (not shown) suggest that they are associated with mesoscale eddies generated along the western flank of the North Atlantic Current in the central Iceland Basin. In Figure 4 the fluctuations visible by altimetry are typically about 50 km wide and have velocities on the order of 0.1 m s^{-1}. Given that eddies in the region are usually ~1,000 m deep (Zhao et al., 2018), this would lead to an ~5-Sv anomaly in transport as each eddy enters at the eastern end of the array. If a similar independent eddy signal of the same size is also occurring at the western end, this would result in an ~7-Sv transport anomaly ($\sqrt{2} \times 5$ Sv) due to eddy noise, which is comparable to the 6-Sv standard deviation of the ERRC transport time series. Therefore, these eddies could explain much of the variation in the ERRC transport.

Individual components of the ERRC (Figure 5) give more insight into the nature of the current. The top two panels of Figure 5 show the baroclinic and barotropic components of the total transport above 1,200 m between moorings M1 and M2, while the third panel displays the transport contributions below 1,200 m

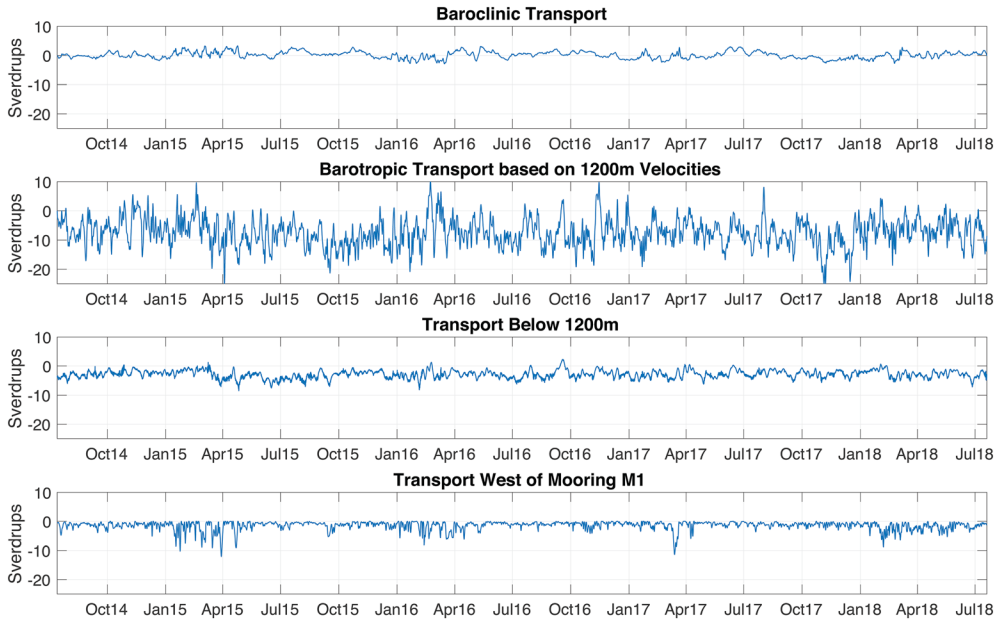

Figure 5. Four years (July 2014 to June 2018) of transport calculations of the different components of the ERRC with a 40-hr low-pass-filter applied. Negative values are in the prevailing direction of the ERRC to the southwest. The first two panels evaluate the ERRC above 1,200 m between moorings M1 and M2. The top panel shows the baroclinic transport while the second panel shows the barotropic transport from the 1,200-m current meters. The third panel displays the transport calculated from current meters below 1,200 m between moorings M1 and M2. The final panel shows additional ERRC transport that extends over the Reykjanes Ridge between IC4 and M1. Mean contributions from each component are 0.1, −7.5, −2.9, and −1.4 Sv (respectively, from top to bottom).

(lighter than $\sigma_\theta = 27.8$ kg m^{-3}) and the fourth panel shows the additional southward transport between moorings IC4 and M1. The baroclinic transport (Panel 1) is the geostrophic transport relative to 1,200 m and the barotropic transport (Panel 2) is the transport-per-unit-depth calculated from the current meters at 1,200 m multiplied by the 1,200-m water column. The ERRC is dominated by barotropic flow with very little contribution from the baroclinic component. This is observed in the velocity profiles as well (Figure 6), as the baroclinic component provides only 0.1 Sv of transport annually. Neither the baroclinic nor barotropic transports between M1 and M2 show a significant seasonal cycle. The transport below 1,200 m appears to contribute a relatively steady 2.9 Sv (Figure 5, Panel 3), while the transport to the west of M1 has a very distinguishable seasonality. This transport only contributes 1.4 Sv in the mean, but surges in transport of up to ~10 Sv are observed during the winter and early spring, which results in a maximum monthly mean transport of 3.0 Sv in March. This phenomenon is often due to a surge in surface-intensified transport near M1 along with a westward extension of the zero-velocity boundary between the ERRC and the northward flowing Irminger Current. While this seasonality does not extend into the overall ERRC transport, some of the strongest synoptic events do seem to lead to an increase in overall transport (e.g., in April 2015 and February 2018 in Figure 3).

In addition to the current meters, transports were also calculated using surface reference velocities derived from altimetry (Figure 7). These transports are only calculated in the top 1,200 m between M1 and M2 to isolate the comparison to the areas where the referencing is applied. Visually, the two time series appear very different mostly due the much higher short-term variability in the current meter-referenced time series; however, there also appears to be little correlation of notably strong or weak events between the two calculations. Indeed, despite the fact that both transports are using the same geostrophic velocities, the overall correlation between the two is low whether low-pass filtering the current meter data to 40 hr (0.17), 10 days (0.20), or 30 days (0.30). The mean transport of each time series is another major discrepancy between the two data sets as the altimeter ADT-derived barotropic transport has a mean of 4.1 Sv while the current meter-derived barotropic transport has a mean of 7.4 Sv. Some of these discrepancies can be explained by the high temporal variability found in the current meter-referenced transport since the ADT-referenced

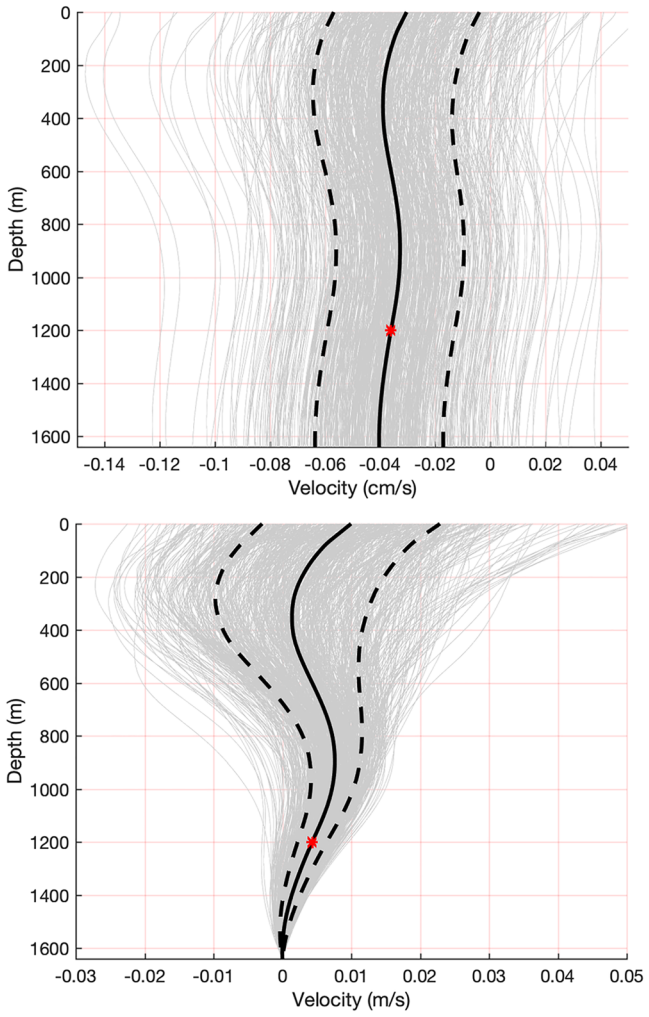

Figure 6. Average absolute velocity profiles (top) and geostrophic velocity profiles (bottom) of the ERRC between moorings M1 and M2. Select individual profiles are shown in gray with a solid black line representing the mean profile and dashed black lines displaying ±1 standard deviation. The red asterisk indicates the reference depth (1,200 m) used in the transport calculations. The figures show the full geostrophic shear profiles to the greatest common depth of moorings M1 and M2 (1,645 m); however, only the transport above 1,200 m is derived from geostrophic shear (referenced to the 1,200-m current meters between moorings M1 and M2); transports below 1,200 (and above $\sigma_\theta = 27.8$ kg m^{-3}) are derived from the full current meter array below 1,200 m (see Figure 2).

transport might miss many of the larger events that occur on timescales of days. Despite the fact that the ADT-merged product is available at daily resolution, spectral analysis (not shown) reveals that the altimetry-derived surface velocities have ~100 times lower power than the current meter-derived surface velocities on time scales of less than 15 days. This means that the altimetry is clearly missing a large portion of the higher-frequency variability that is reflected in the current meter based times series. However, the current meter-referenced time series also has several longer time intervals of consistent large volume transport (September–November 2015, June–July 2016, and November–December 2017) that are not reflected in the ADT-referenced time series and cannot be explained by the current's variability. Given the high accuracy and fast collection rate of the current meters, this suggests that the ADT-referenced transport may be underestimating the true transport of the ERRC, possibly due to errors in estimates of the geoid over the rough topography (Rio et al., 2011) near the Reykjanes Ridge, as well as to the temporal and spatial smoothing inherent in the merged altimetry data set.

As was the case in the overall transport, synoptic transport estimates from shipboard data is again used to compare with both transport time series over the same section (Figure 7). While the synoptic estimates tend to compare better with the current meter based time series than the altimetry based time series, there are not enough realizations to say with statistical confidence which is more accurate, particularly with regard to the mean transport difference. Still, we believe the current meter based transport is more accurate given its coincident direct measurements and good overall agreement with the available simultaneous synoptic estimates, pending confirmation of the 2018 and future synoptic comparisons.

3.2. ERRC Pathways and Volume Transport

To understand the broader development of the East Reykjanes Ridge Current, altimetry and Argo data are used to evaluate the current's pathways. Figure 8 shows velocity vector plots of flow at the surface derived independently from altimetry and Argo, along with velocities at 1000 m depth from Argo drift data. The Argo-derived surface velocities shown in Figure 8 (middle) were calculated from the gridded Argo T/S profile data to determine surface geostrophic velocities relative to 1,000 m, which were then referenced to the Argo absolute drift data at 1,000 m. The surface images illustrate two dominant branches of flow entering the Iceland Basin: a western branch near 27°W that continues to flow northward in the central Iceland Basin and an eastern branch near 23°W that impinges on the southern edge of the Hatton-Rockall Plateau. Argo water mass analysis of these two flows (not shown) indicate that much of this water is relatively fresh recirculated subpolar gyre water, as the western branch contains some of the freshest surface waters found in the basin (<34.92 psu) and the eastern branch only shows the influence of higher salinity subtropical waters (>35.3 psu) on its eastern edge. Altimetry suggests that these waters mostly originate from the northern branch of the North Atlantic Current, which recirculates fresh subpolar gyre waters from the Labrador Sea (Yashayaev et al., 2007; Yashayaev & Clarke, 2008). The majority of saltier North Atlantic Current waters that enter along the eastern side of the basin are supplied through a smaller flow at 20°W and from a northward flow in Rockall Trough near 16°W that retroflects westward around the southern edge of the Rockall Bank. These waters move northward in the basin mainly within the Hatton Bank Jet (Houpert et al., 2018) along the western flank of Hatton Bank. Substantial mixing occurs between the Hatton Bank Jet and the two branches of recirculated subpolar gyre water as they move northward due to the high levels of eddy energy in the region and the presence of several semipermanent eddies (Read &

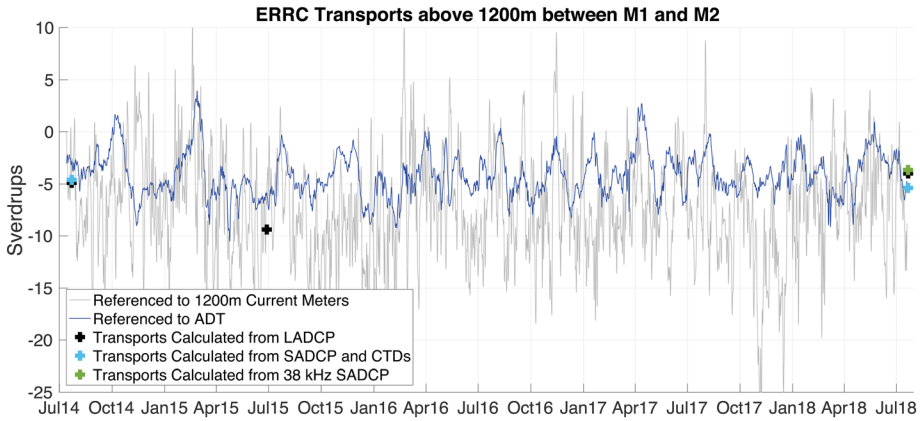

Figure 7. ERRC transports above 1,200 m between moorings M1 and M2 referenced to altimetry (blue) and OSNAP current meters (gray). Negative values are in the prevailing direction of the ERRC to the southwest. Crosses indicate synoptic transport estimates using LADCP (black), combined SADCP with geostrophic shear (aqua), and low frequency SADCP (green) from cruises.

Pollard, 2001; Wade & Heywood, 2001). Near 60°N, some of the waters in the Hatton Bank Jet veer offshore to merge with the northward flowing subpolar gyre water in the central Iceland Basin, leading to about 7 Sv of mixed subtropical/subpolar waters within the top 2,000 m flowing through the section labeled "B" in Figure 8. Both the altimetry and Argo surface velocity maps (Figure 8) suggest that a significant portion of this flow then retroflects westward along the Icelandic Slope to form the surface origins of the ERRC. Both maps also indicate that a portion of the Hatton Bank Jet later veers westward near 62°N along the southern edge of the Iceland-Faroe Ridge to possibly supply additional waters to the ERRC, although the altimetry data suggest that much of this water ultimately flows northward across the Iceland-Faroe Ridge into the Norwegian Sea.

At 1,000 m (Figure 8, bottom), the Argo drift data suggest that the formation of the ERRC at intermediate depths occurs along the Iceland-Faroe Ridge in the northeast corner of the Iceland Basin. This slope-intensified flow of 5.5 Sv moves along the Icelandic slope (Section A) and combines with the previously discussed retroflected surface-intensified flow from the central Iceland Basin near Section C. In Figure 9, we show the derived geostrophic velocity sections across each of the labeled sections in Figure 8, illustrating the surface-intensified North Atlantic Current flow across Section B and the bottom-intensified flow across Section A. The convergence of these two flows at Section C has a total transport of 12.8 Sv based on Argo profile data referenced to Argo 1,000-m drift, while the Argo data referenced to altimetry shows a transport of less than half that strength (6.3 Sv). In fact, the altimetry-referenced Argo data consistently produces weaker transports than the Argo-only data throughout much of the ERRC's domain (by ~1–6 Sv; compare insets of Figures 8), which we believe is due to an underestimate of transport from altimetry as noted in the previous section. In what follows we therefore focus our discussion mainly on the Argo-derived transports, although estimates from both methods are listed on their respective images in Figure 8.

Downstream of Section C, the ERRC flow continues to follow the bathymetry at a nearly steady intensity of 10–12 Sv as it turns to the southwest and follows along the eastern flank of the Reykjanes Ridge through Sections D–F. Upon reaching Section G—the OSNAP line—there is a notable decrease in transport down to 6.5 Sv due to some recurvature of the flow over the ridge into the Irminger Basin. Despite continued flow over the ridge downstream of Section G, the transport slightly increases at Section H (7.1 Sv) due to an influx of recirculated subpolar gyre water entering from the south near 57°N, 29°W and then retroflecting in the direction of the ERRC to the southwest. Uncertainties in the Argo-derived transports include the uncertainty in baroclinic transport for each section (based on standard errors of the mean Argo T/S profiles used in the geostrophic calculations) and the uncertainty in the 1,000-m reference velocities based on standard errors of the gridded Argo drift data. The uncertainties in the Argo-based transports are typically on the order of ~1–2 Sv (Figure 8), while those based on the altimetry surface ADT reference velocity are generally slightly smaller due to the larger averaging period available for the ADT data (1993–2018) versus that for the 1,000-m Argo drift data (2004–2016).

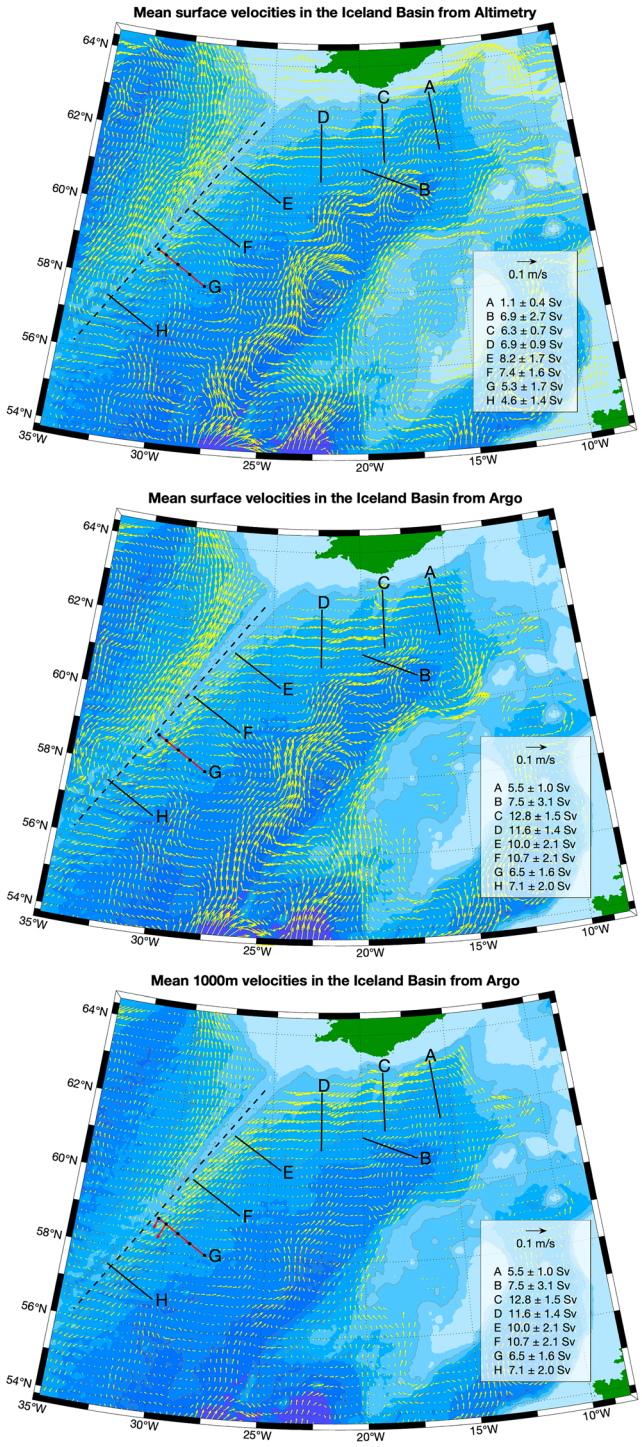

Figure 8. Circulation in the Iceland Basin as determined by surface altimetry data (top), Argo surface geostrophic velocities referenced to 1,000-m Argo drift data (middle), and 1,000-m Argo drift data (bottom). Section locations A–H analyzed in this study are labeled and denoted by black lines, except for the location of the OSNAP line—Section G—which is indicated by a red line with United States-supported OSNAP mooring locations marked by black points. The dashed line notes the location of the Reykjanes Ridge section shown in Figure 10. Bathymetry is noted by color shading in 500-m increments. The red vectors on Section G in the bottom panel show the 1,200-m mean velocities from 4 years of current meter data at all five United States-supported OSNAP moorings. Insets in each panel show the transport values and standard errors calculated either exclusively from Argo data (middle and bottom) or from a combination of Argo and altimetry (top); transport values and errors include all waters above 2,000 m that are lighter than $\sigma_\theta = 27.8$ kg m^{-3} and flowing across each section in the prevailing direction of the ERRC.

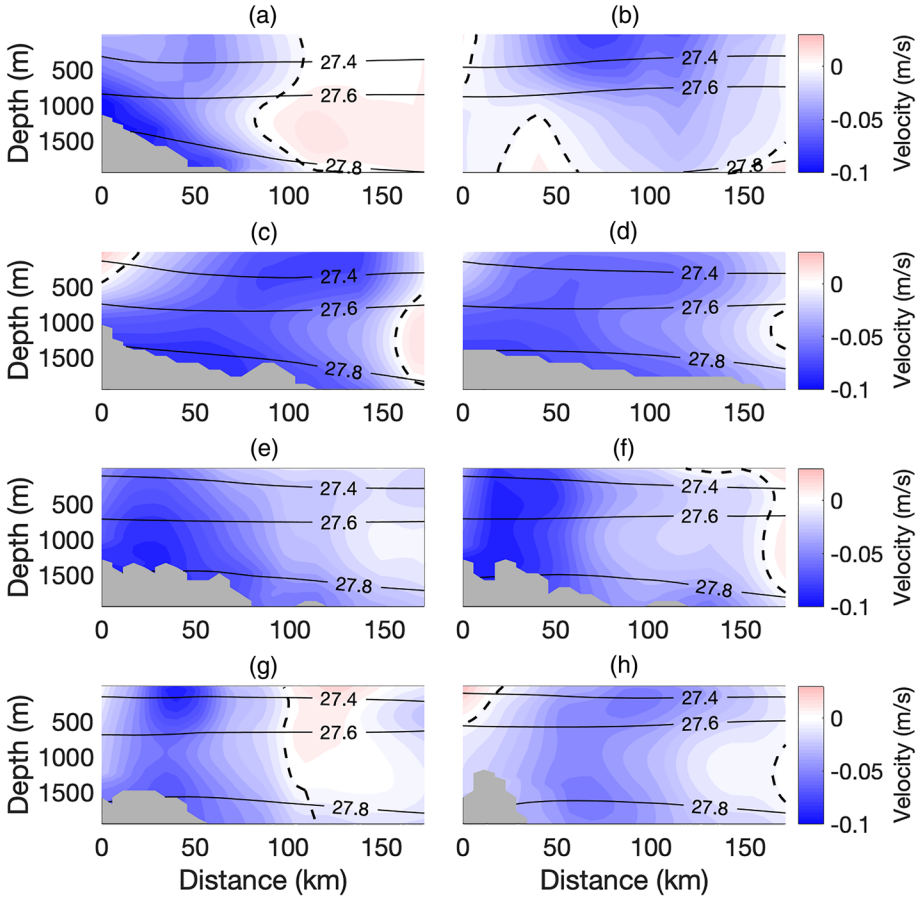

Figure 9. Cross-sectional velocity images of eight sections (A–H) of the ERRC as labeled on Figure 8, derived from Argo geostrophic shear and 1,000-m drift data. Negative values are in the prevailing direction of the ERRC at each location. Isopycnals (σ_θ) are labeled in black. The domain used in the Argo transport calculations of the ERRC (Figure 8, insets) is denoted by thick dashed black lines (where applicable), which always corresponds to the zero-velocity contour with the exception of the bottom of Section G. Bathymetry is indicated in gray. Section G is the location of the OSNAP line.

Notably, the Argo transport estimate at the OSNAP line (6.5 Sv) is nearly 50% weaker than our direct estimate from the moored OSNAP observations (11.7 Sv). This is mostly due to weaker velocities at depth in Argo. The 4-year mean velocities from the five 1,200-m current meters (Figure 8c in red) show a significantly more intense flow at M1 (0.07 m s^{-1}) and D1 (0.11 m s^{-1}) than Argo inferred to the same depth and locations (0.02 and 0.06 m s^{-1}, respectively). Interestingly, upstream of this section the Argo data is in closer agreement with the mean OSNAP mooring data, showing that the ERRC is a weakly bottom-intensified current (Figure 9: Sections D–F) with 1,000+-m velocities similar to the OSNAP results (~0.09 m s^{-1}). Mean surface velocities from altimetry comparing the Argo time period (2004–2016) to OSNAP (2014–2018) do not suggest that different collection periods are responsible for these differences, though they could be due to the limitations in Argo sampling as Section G is near a region of poor coverage (not shown).

To observe the transition of the ERRC into the Irminger Basin, full-depth velocity profiles were created along the axis of the Reykjanes Ridge (Figure 10, top). Here we use Argo data referenced to altimetry in order to extend the analysis to shallower terrain where Argo drift data is limited. Upstream of Section F, the ERRC has leakage of 2.6 Sv at 0.01–0.02 m s^{-1} over the ridge, but the majority of the flow stays trapped against the eastern flank of the topography. Near 59.8°N, approximately 120-km upstream of the OSNAP line (Section G) is the start of an observed pathway over the ridge. This pathway ends about 60 km downstream of the OSNAP line—near 58.5°N—where the flow encounters a weak counter current at depth. This 180-km section accounts for 5.4 Sv of transport into the Irminger basin, and the net cross-ridge flow

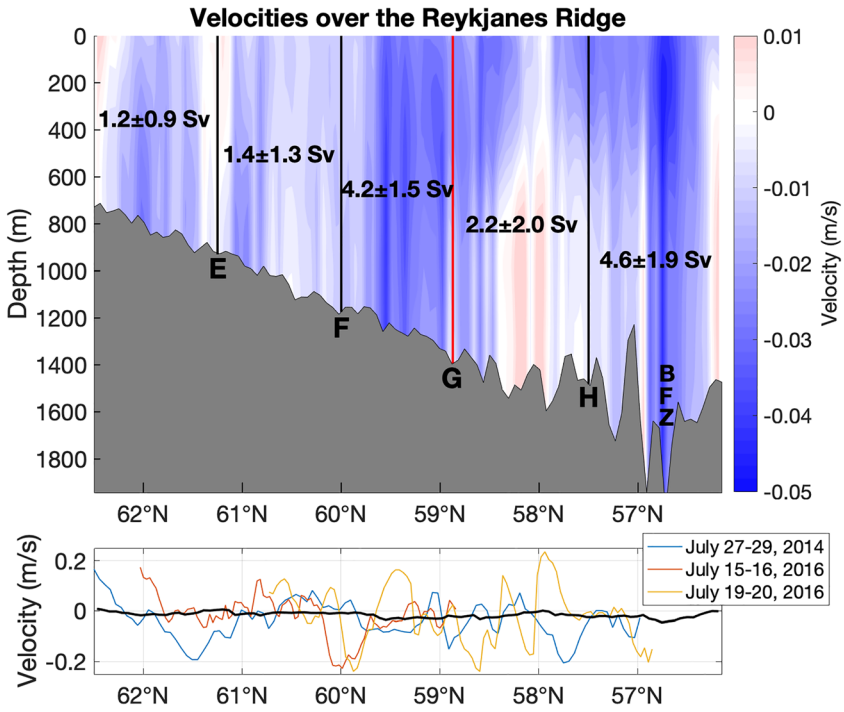

Figure 10. Top: Mean velocities over the Reykjanes Ridge calculated from combined Argo and altimetry with negative values in blue corresponding to westward flow over the ridge. This section is marked by the dashed line in Figure 8. The locations where the other sections shown in Figure 8 intersect the ridge are indicated, including Section G—the OSNAP line—which is marked in red. Mean transport estimates and their standard errors for the cross-ridge flow between sections are noted on the figure. BFZ denotes the location of the Bight Fracture Zone. Bottom: Top 500-m mean velocities from shipboard ADCP data from OSNAP cruises along corresponding portions of the ridge, with the overall top 500-m climatological velocity mean from the top image shown in black.

between Sections F and H is 6.4 Sv. An additional pathway of about 3.5 Sv of flow is also observed downstream of Section H over the Bight Fracture Zone between two faint bottom-intensified counter currents. Synoptic ADCP cruise data (Figure 10, bottom) along the section illustrates the importance of using time mean data in this analysis. While the 2016 data support the existence of a cross-ridge pathway downstream of Section H and a pathway close to Section F, there are large variations in the three synoptic realizations and each of them shows notable differences from the much weaker mean flow derived from Argo/altimetry. In fact, the two 2016 sections were observed only a few days apart and yet show some remarkable differences.

Evidence suggests that the cross-ridge pathway located primarily between Sections F and G is where the ERRC begins to terminate as a quasi-boundary flow and turn westward across the Reykjanes Ridge into the Irminger Current. Why this happens at this particular location is not clear, but it likely has to do with the decreasing topographic constraint of the Reykjanes Ridge on the ERRC, as the height of the ridge decreases to the southwest. Since the ERRC is quasi-barotropic, its ability to turn over the ridge should be related to the amount of columnar stretching required to cross it. To investigate this, we calculated the difference between the mean depth under the core of the ERRC as it flows along the eastern flank of the RR and the height of the RR at the same latitudes. From Sections D to G (approximately 61.5°N to 58.5°N; see Figure 8), the ERRC flows in depths from about 1,400 to 1,600 m (shifting slightly to deeper isobaths along its path), while the height of the RR decreases from about 900 to 1,400 m over the same distance. The difference of these two heights (ΔH) relative to the mean depth below the core of the ERRC (H) progressively decreases from ~0.35°N at 61°N to less than 0.2 near 59.5°, suggesting that a threshold value of ΔH/H of ~0.2 is a where a substantial part of the ERRC can begin to cross the ridge.

Surface velocity vector plots (Figure 8) show some addition of flow to the ERRC near this location by recirculated subpolar gyre water entering from the south near 57°N, 29°W. This new flow soon turns to the west

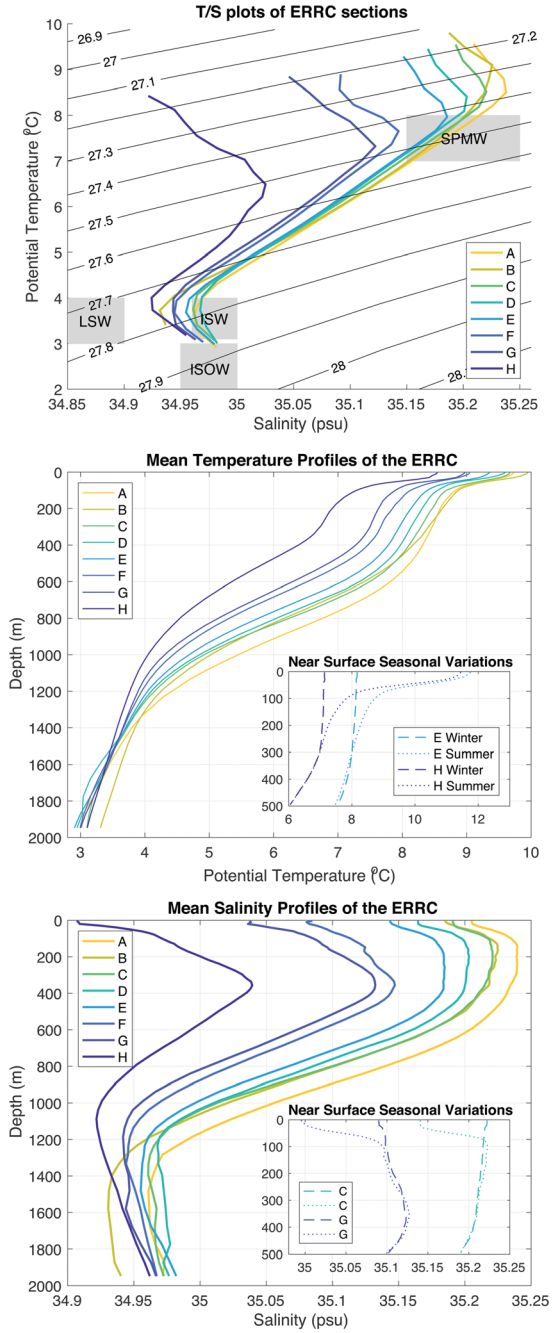

Figure 11. Mean temperature-salinity diagrams (top), temperature profiles (middle), and salinity profiles (bottom) from Argo data of eight sections of the ERRC as displayed in Figure 8. Plots include all water within the domain of the ERRC. Insets in temperature and salinity figures display summer (July–September) and winter (January–March) means from sample sections with dotted and dashed lines, respectively. Gray lines represent isopycnals (σ_θ) and gray boxes denote the core water properties of different water masses found in the Iceland Basin (top). Acronyms and water mass property references are as follows: Subpolar Mode Water (SPMW; Brambilla & Talley, 2008); Labrador Sea Water (LSW; Fogelqvist et al., 2003; van Aken & de Boer, 1995; Zhao et al., 2018); Icelandic Slope Water (ISW; Read, 2000; van Aken & de Boer, 1995); Iceland Scotland Overflow Water (ISOW; Fogelqvist et al., 2003; van Aken & de Boer, 1995).

and then the southwest, essentially extending the ERRC south of Section H. The location of the velocity core (Figure 9) relative to the ridge also suggests a different flow is observed at Section H; Sections C–G depict the ERRC as a ridge-hugging boundary current of >0.08 m s^{-1} in the core, while Section H shows a weakened flow with a maximum velocity of 0.05 m s^{-1} located off the ridge. Water mass analysis from Argo (Figure 11) supports this analysis as significant freshening occurs from Section G to Section H, which suggests that much of the extended ERRC flow at Section H must have come from the recirculated subpolar gyre flow. South of Section H, the surface velocity maps from Argo and altimetry differ, with the altimetry data suggesting that most of the surface ERRC turns westward into the Irminger Basin by ~56°N while the Argo maps show a weaker extension of the ERRC along the eastern flank of the RR to at least 54°N, at both the surface and 1,000 m.

In order to quantify the lateral inputs of recirculated gyre water between sections, Figure 12 shows the transport budget in the top 2,000 m along the eastern flank of the Reykjanes Ridge. All transports are derived exclusively from Argo, except those over the ridge which use altimetry as a surface reference, as noted above. From Sections E to H, approximately 3 Sv flows into each region from the inner Iceland Basin, totaling 8.2 Sv, while a similar total transport (7.8 Sv) exits over the ridge into the Irminger Basin. Overall, 9.0 Sv flows across the entire length of the resolved Reykjanes Ridge section from Iceland to Section H and is balanced by a net flow of the same amount (9.0 Sv) from the Iceland basin into the ERRC between Sections D and H. The inclusion of these lateral flows generally balances the mass well in each box, with transport imbalances of mostly ~1 Sv or less. The largest transport discrepancy, of 3.3 Sv between Sections F and G, is due to the abrupt drop in the ERRC transport between these sections, which we believe may be due to an underestimate the ERRC transport at Section G derived from Argo relative to our mooring data.

3.3. ERRC Water Mass Structure and Along-Stream Changes

Annual mean temperature and salinity data of the ERRC at each section, and associated θ/S plots (Figure 11), illustrate the water mass properties of the ERRC and how they evolve as the current transits around the basin. A deep winter mixed layer of 300–400 m (Figure 11 middle, inset) creates a year-round salty Subpolar Mode Water lens that can extend beyond 500 m in the core of the ERRC (Figures 2 and 11 bottom). This water mass, formed from Modified North Atlantic Water, wraps cyclonically all the way around the northern rim of the Iceland basin and imprints its salty signature on the near-surface waters of the ERRC, relative to the fresher waters found in the central Iceland basin (Brambilla & Talley, 2008). At intermediate depths, modified Labrador Sea Water from the central Iceland Basin mixes into the ERRC, which leads to a salinity minimum at potential temperatures of between 3.7–4.0°C in each of the sections (Figures 2 and 11 top). The majority of the ERRC is a mixture of these two water masses—Subpolar Mode Water and modified Labrador Sea Water—at depths shallower than ~1,400 m. At the bottom of the profiles, near 2,000 m, the θ/S properties tend toward the characteristics of Iceland Scotland Overflow Water, which fill the deepest layer of the Iceland Basin along the Reykjanes Ridge. The saltier signature of this water mass results from the mixing of Subpolar Mode Water into the cold, dense waters that

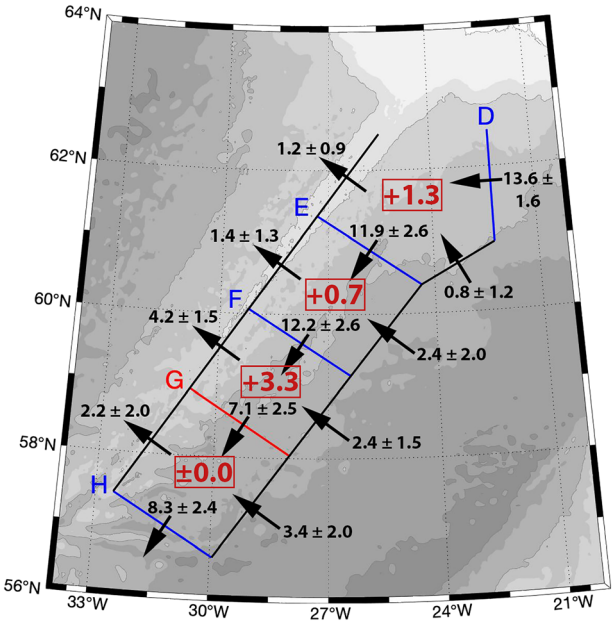

Figure 12. Net transport budget (with standard errors) of all waters in the top 2,000 m along the eastern flank of the Reykjanes Ridge. Sections from Figure 8 are indicated in blue, with Section G—the OSNAP line—marked in red. Boxed values in red indicate the transport surplus or deficit in each region. Bathymetry is noted by gray shading in 500 m increments. All transports are estimated exclusively from Argo, except transport estimates on the Reykjanes Ridge, which use altimetry as a surface reference velocity. Transports are in Sverdrups.

spill across the Norwegian Sea sills into the Iceland Basin (Beaird et al., 2013). At depths below the salinity minimum and above the Iceland Scotland Overflow Water layer, the ERRC contains Icelandic Slope Water, which is slightly warmer than Iceland Scotland Overflow Water and also contains a salty imprint from entrained Subpolar Mode Water (Beaird et al., 2013).

As the sections progress along the Icelandic slope, a gradual surface-intensified cooling and freshening is observed through Section E. The transition from Section E to Section F shows a more pronounced freshening due to an input of recirculated subpolar gyre water near 60°N, 26°W. At Section G—the OSNAP line—the cooling and freshening trend continues before an even stronger freshening and cooling increase is observed at Section H. This significant change in properties in the upper water column from Section G to Section H (>0.13 psu, 1°C) is further evidence that the main core waters of the ERRC originating from the NAC have largely passed over the ridge upstream of Section H and are replaced by recirculating subpolar gyre water from the central Iceland Basin.

All profiles show a subsurface surface salinity maximum which is caused by excess precipitation over evaporation in the region shown in surface reanalysis products (e.g., ERA-5 produced by the European Centre for Medium-Range Weather Forecasts, https://www.ecmwf.int/en/forecasts/datasets/reanalysis-datasets/era5), and this continuous input of freshwater leads to an increasing difference between the surface salinity and the salinity maximum progressing southwestward along the current. The salinity maximum also deepens with this progression from about 160 m at Section B to about 350 m at Sections F–H. This transition includes a 100 m deepening from Section E to Section F as surface-intensified recirculated subpolar gyre water near 60°N, 26°W begins to contribute to the ERRC.

Temperature profiles show a gradual cooling of the ERRC that can be attributed to both surface heat loss and mixing with the cooler recirculated subpolar gyre waters. Seasonal variations in temperature (Figure 11 middle, inset) show an ~300-m winter mixed layer, while the stratified ocean in the summer results in a warm water cap in the top ~50 m. The seasonal variations in salinity show a similar behavior (Figure 11 bottom, inset), with a mostly homogenous mixed layer in the winter but a fresher surface cap in the top 50–100 m due to greater isolation of excess P-E to the surface layer in the stratified summer season.

To evaluate these property changes in density space, the flow-weighted density was calculated along each section of the ERRC within the domain as

$$\frac{\iint \rho v \, dxdz}{\iint v \, dxdz}$$

where ρ is potential density (kg m^{-3}) and v is the velocity (m s^{-1}) through each section. Combining Sections A and B as the formation waters of the ERRC yields a flow-weighted density of 27.53 kg m^{-3}. By the time the ERRC reaches the OSNAP line, the flow-weighted density has increased to 27.61 kg m^{-3}. This change of 0.08 kg m^{-3} is notable when considering the flow-weighted density change of the entire AMOC is 0.31 kg m^{-3} (F. Li, personal communication, 31 January 2020). The change in flow-weighted density of the ERRC is almost entirely due to cooling and freshening by surface processes along its path, since the density of recirculated subpolar gyre waters from the interior Iceland Basin and the outflow over the ridge upstream of the OSNAP line have a similar average density and contribute negligibly to the overall density change of the ERRC. Although the ERRC is only one of many components of the AMOC system, the relatively large density change along its path illustrates the important role that progressive water mass modification plays in the boundary current system of the subpolar gyre, as warm and salty

surface waters are gradually transformed into denser waters that form the deep limb of the MOC. The ERRC can effectively be considered the first step in this process for the NAC waters that recirculate in the subpolar gyre rather than crossing the Iceland-Faroe Ridge into the Norwegian Sea.

4. Discussion and Conclusion

The East Reykjanes Ridge Current (ERRC) originates at the northern end of the Iceland Basin due to the convergence of several flows. At the surface, altimetry and Argo analysis suggest that the ERRC is formed mainly from the northern branch of the North Atlantic Current that enters the Iceland Basin near 24°W (Figure 1). This source slightly differs from Daniault et al. (2016; Figure 1) who attribute the main northward flow in the center of the Iceland Basin to the middle branch of the North Atlantic Current. However, the northward flow in the central Iceland Basin is relatively fresh (~34.9–35.0 psu), suggesting that it derives from modified Labrador Sea Water in the northern branch of the North Atlantic Current. Additions to this flow from an extension of the middle branch of the North Atlantic Current near 55°N and 60°N increase its salinity (~35.2 psu) before it reaches the Icelandic slope. Argo data suggest that a portion of the middle branch extension also wraps its way around the western side of the Hatton Bank and continues cyclonically along the edge of the Iceland Basin as an additional contribution to the formation of the ERRC. This is observed near the 50 km location in Section A of Figure 9. Despite its more circuitous path around the subpolar gyre, these are the most saline waters to contribute to the ERRC (Figure 11).

The lower part of the ERRC originates from modified Iceland Scotland Overflow Water known as Icelandic Slope Water (Read, 2000; van Aken & de Boer, 1995). The main mass of Iceland Scotland Overflow Water originates as Norwegian Sea Deep Water and Norwegian Sea Arctic Intermediate Water which overflow into the Iceland Basin through the Faroe Bank Channel and entrain Subpolar Mode Water (Beaird et al., 2013). While much of this water descends into the basin from the channel outflow, another portion remains along shallower topography on the southern side of the Iceland-Faroe Ridge where it is modified by diapycnal mixing with recirculating Subpolar Mode Water and modified Labrador Sea Water (Beaird et al., 2013; Brambilla & Talley, 2008; van Aken & de Boer, 1995; Yashayaev & Dickson, 2008). Additional Norwegian Sea Deep Water and Norwegian Sea Arctic Intermediate Water overflow occurs over the Iceland-Faroe Ridge, as well as a contribution from the fresher and slightly warmer Modified East Icelandic Water (Beaird et al., 2013; Hansen & Østerhus, 2000). Through these contributions and modifications, these waters become Icelandic Slope Water, which primarily differentiates itself from typical Iceland Scotland Overflow Water (2.7–2.9°C) by its warmer temperatures. Argo observations of this water mass show very similar characteristics (3.9–4.3°C, 34.98–35.00 psu) to those described in previous studies (Read, 2000; van Aken & de Boer, 1995). Therefore, we conclude that it is the confluence of these two sources—the surface-intensified North Atlantic Current waters that enter the Iceland Basin from the south, and the Icelandic Slope Water that is formed at intermediate depths along the southern Iceland-Faroe Ridge slope—that give the ERRC its quasi-barotropic structure. Although some deepening of the velocity structure of the parent North Atlantic Current flow might be expected due to deep wintertime mixing along its pathway to the ERRC as it transforms into Subpolar Mode Water (Brambilla & Talley, 2008; de Boisseson et al., 2012; Thierry et al., 2008), it is fundamentally the addition of these Icelandic Slope Waters to the ERRC that lead to the nearly barotropic, or in some cases bottom-intensified, nature of the current.

From its origin, the ERRC maintains a relatively steady mean transport along the Iceland Shelf and southwestward along the eastern flank of the Reykjanes Ridge until it passes 60°N near Section F. While the intensities differ between Argo-derived estimates (10–13 Sv) and altimetry derived estimates (6–8 Sv), both show a notable decrease in transport by the time they reach the OSNAP line at Section G (6.5 Sv and 5.3 Sv, respectively) due to part of the ERRC retroflecting over the Reykjanes Ridge into the Irminger Basin, even though OSNAP results at this location still show an ERRC transport of 11.7 Sv. For comparison, Petit et al. (2019) found a transport of 13.8 Sv for the ERRC from synoptic cruise data near the OSNAP line and also found a lower transport value upstream where the ERRC transitions from the Iceland Shelf to the Reykjanes Ridge near 62°N (10.6 Sv). The increased transport between the two sections in Petit et al.'s (2019) study was the result of an additional westward transport of 15.9 Sv entering the ERRC from the Iceland Basin with 13.8 Sv of it crossing over the ridge upstream of the OSNAP line, while the time mean Argo analysis presented here have notably weaker transports over similar sections (5.6 and 6.8 Sv, respectively). As for

the two branches of the ERRC found by OVIDE (Daniault et al., 2016), OSNAP cruise hydrography and Argo analysis used in this study did not clearly indicate the smaller surface-intensified offshore branch of the ERRC. The only relevant similar feature found in the area is the recirculating flow from the Iceland Basin that this study theorizes partially replaces the ERRC near 57°N, 29°W.

The primary pathway of the ERRC over the Reykjanes Ridge into the Irminger Basin presented in this analysis near 59°N has been observed in other recent studies (Daniault et al., 2016; Lherminier et al., 2010; Petit et al., 2018, 2019). An additional pathway to the south (Figure 10) is also observed in three of these studies (Daniault et al., 2016; Petit et al., 2018, 2019) with the analyses by Petit et al. (2018, 2019) most closely matching the location of our pathway over the Bight Fracture Zone at 57°N. At depth, a numerical model of Iceland Scotland Overflow Water (Xu et al., 2010) found pathways at the same two locations as our analysis. Even though Iceland Scotland Overflow water is excluded from this study, the barotropic nature of the cross-ridge flow (Figure 10) suggests most water masses transition to the Irminger Basin at similar locations. Petit et al. (2018, 2019) and Daniault et al. (2016) additionally report a surface pathway near 62°N. A schematic in the Petit et al. (2019; Figure 7) study in particular notes a greater transport at the 62°N location (>7 Sv) than the pathways at 57°N and 59°N (both 6.7 Sv) though other results in the paper attribute that transport more to the accumulation of leakage over a long distance (~500 km) than to a specific pathway. While this study does not find significant flow across the ridge near 62°N (~1 Sv; Figure 10), the other two estimates generally agree with our Argo/altimetry combined calculations (5 and 7 Sv, respectively). Chafik et al. (2014) also conducted a time mean analysis from altimetry in the region and found very little transport crossing the ridge north of 60°N. The methods used in these studies, including the present study, have a number of limitations. In the case of Petit et al. (2018, 2019) and Daniault et al. (2016), their results are based on synoptic data from a single cruise (or limited number of cruises) in a region of high variability. In Chafik et al. (2014) and this study, the rough topography near the ridge likely leads to greater errors from altimetry due to uncertainties in the geoid (Rio et al., 2011). Additionally, Argo drift data used in this study does not directly measure velocity over the ridge north of ~60°N due to the shallow topography.

The results presented in this study indicate that the East Reykjanes Ridge Current (ERRC) is a highly variable flow of about 12 Sv that originates along the Iceland slope in the northern Iceland Basin and terminates near the OSNAP line at 58°N. Our transport estimate along the OSNAP line, derived from dynamic height moorings referenced to deep current meter measurements, is larger than that derived using altimetry as a surface reference or from Argo data at the same location but is similar to recent estimates from in situ observations (Petit et al., 2019). However, the Argo estimates at several upstream sections within the ERRC are closely comparable to our estimates along the OSNAP line. While it could be expected that altimetry would underestimate the variability of the ERRC due to inherent temporal and spatial smoothing (e.g., Figure 7), it is not clear why altimetry should lead to an underestimate of the mean ERRC transport. Indeed, surface velocities across most of the domain of the ERRC derived from altimetry are lower than those derived from Argo with subsurface (1,000 m) Argo drift reference (Figure 8). We speculate that inaccuracies in the geoid or other factors entering into the determination of the mean dynamic topography over the rough topography of the Reykjanes Ridge may be the cause of this bias.

The high degree of variability of the ERRC—also underestimated especially on shorter time scales by altimetry—can be ascribed in part to mesoscale eddies passing through the array, but may also be due to the particular location of the OSNAP Array relative to the termination point of the ERRC. As shown in the Argo and altimetry data (Figures 8 and 10), the OSNAP Array lies in the vicinity of a significant cross-ridge pathway for ERRC waters into the Irminger Basin, and meandering of this cross-ridge pathway to the north or south of the array could lead to enhanced variability of the ERRC transport at this location.

Along its path, the ERRC freshens and cools, which, despite its comparably small geographic domain (a total length of some 900 km from its origin south of Iceland to its termination south of the OSNAP line), leads to a significant increase in its flow-weighted density of 0.08 kg/m^3. This is accomplished mainly by cooling of the ERRC flow of ~1°C, though this is slightly offset by a freshening of ~0.05–0.1 psu (Figure 11). As noted above, the buoyancy loss occurring along the ERRC's path in the Iceland Basin is about one fourth of the total buoyancy loss associated with the AMOC in the subpolar North Atlantic, expressed in terms of the flow-weighted density difference between the upper and lower limbs across the OSNAP line. Since some of the upper limb waters cross the Iceland-Faroe Ridge and are directly

transformed into overflow waters in the Norwegian Sea, a more relevant measure of the importance of buoyancy loss in the ERRC is to compare it to the net buoyancy loss of upper ocean waters as they circulate along their cyclonic pathway around the subpolar gyre. Besides the ERRC, the cyclonic boundary current system of the subpolar gyre includes the Irminger Current, East Greenland Current, West Greenland Current, and finally the Labrador Current, which is adjacent to the Labrador Sea where the final stage of intermediate depth convection occurs into the AMOC's lower limb. Based on historical data from the Labrador Sea (Yashayaev, 2007; Yashayaev & Loder, 2016), the average potential density of postwintertime convected waters is approximately 27.77 kg/m^3 (T ~ 3°C, S ~ 34.84 psu), which is a net change of 0.24 kg/m^3 relative to the flow weighed density of the headwaters that form the ERRC (27.53 kg/m^3). Therefore, about one third of the net density change around the rim of the subpolar gyre from the northern Iceland Basin to the Labrador Sea occurs in the ERRC. While there is additional cooling between the ERRC and Labrador Sea of about 2.5°C (the flow-weighted temperature of ERRC at the OSNAP line is ~5.5°C), it is offset by large atmospheric and Arctic freshwater inputs to the system along this pathway, making the density change occurring within the ERRC a relatively large component of the net density change of the waters circulating within the subpolar gyre.

The OSNAP measurements are continuing beyond the 4-year period studied here, and since 2018, the moored observations at the deep moorings D1, D2, and D3 have been extended upward to include measurements through the whole water column with additional current meters and ADCPs. Therefore, more observations will be forthcoming to better resolve the structure and variability of the ERRC. Nevertheless, these initial observations of the ERRC have provided the first direct in situ time series of the current, and together with Argo and altimetry data have provided a baseline description of the ERRC and its evolution within the Iceland Basin. Future results will contribute to the study of interannual variability in the AMOC and its evolution in a changing climate, and the role played by the ERRC in the variability of the overall subpolar gyre circulation.

Data Availability Statement

OSNAP data used in this study are available online (at https://www.o-snap.org/oberservations/data/).

Acknowledgments

The authors would like to thank the captains and crews of the R/V Knorr, R/V Pelagia, RRS Discovery, and R/V Neil Armstrong for their hospitality aboard their vessels and for helping to ensure the completion of this research. We would also like to thank Dr. Femke de Jong and the Royal Netherlands Institute for Sea Research for access to data from their eastern most mooring (IC4) along the OSNAP line. We would like to acknowledge Dr. Tiago Biló for the help with the Argo-based North Atlantic climatological mean absolute geostrophic velocity profiles. These data can be found in the University of Miami's Scholarly Repository at https://doi.org/10.17604/cf5z-x124. Finally, we would like to thank the National Science Foundation for funding this research through grants OCE-1259398 and OCE-1756231.

References

Beaird, N. L., Rhines, P. B., Eriksen, C. C., Beaird, N. L., Rhines, P. B., & Eriksen, C. C. (2013). Overflow waters at the Iceland–Faroe Ridge observed in multiyear seaglider surveys. *Journal of Physical Oceanography*, *43*, 2334–2351. https://doi.org/10.1175/JPO-D-13-029.1

Bilo, T. C. (2019). North Atlantic observed climatological mean absolute geostrophic velocity profiles. University of Miami Libraries. https://doi.org/10.17604/cf5z-x124

Bilo, T. C., & Johns, W. E. (2019). Interior pathways of Labrador sea water in the North Atlantic from the Argo perspective. *Geophysical Research Letters*, *46*(6), 3340–3348. https://doi.org/10.1029/2018GL081439

Brambilla, E., & Talley, L. D. (2008). Subpolar mode water in the northeastern Atlantic: 1. Averaged properties and mean circulation. *Journal of Geophysical Research*, *113*, C04025. https://doi.org/10.1029/2006JC004062

Chafik, L., Rossby, T., & Schrum, C. (2014). On the spatial structure and temporal variability of poleward transport between Scotland and Greenland. *Journal of Geophysical Research: Oceans*, *119*, 824–841. https://doi.org/10.1002/2013JC009287

Daniault, N., Mercier, H., Lherminier, P., Sarafanov, A., Falina, A., Zunino, P., et al. (2016). The northern North Atlantic Ocean mean circulation in the early 21st century. *Progress in Oceanography*, *146*, 142–158. https://doi.org/10.1016/J.POCEAN.2016.06.007

de Boisseson, E., Thierry, V., Mercier, H., Caniaux, G., & Desbruyeres, D. (2012). Origin, formation and variability of the Subpolar Mode Water located over the Reykjanes Ridge. *Journal of Geophysical Research*, *117*, C12005. https://doi.org/10.1029/2011JC007519

Dickson, R., & Brown, J. (1994). The production of North Atlantic Deep Water: Sources, rates, and pathways. *Journal of Geophysical Research*, *99*(C6), 12,319–12,341. https://doi.org/10.1029/94JC00530

Emery, W. J., & Thomson, R. E. (2001). *Data analysis methods in physical oceanography*. Amsterdam, the Netherlands: Elsevier.

Fogelqvist, E., Blindheim, J., Tanhua, T., Osterhus, S., Buch, E., & Rey, F. (2003). Greenland-Scotland overflow studied by hydro-chemical multivariate analysis. *Deep-Sea Research Part I: Oceanographic Research Papers*, *50*(1), 73–102. https://doi.org/10.1016/S0967-0637(02)00131-0

Hansen, B., & Østerhus, S. (2000). North Atlantic-Nordic Seas exchanges. *Progress in Oceanography. Pergamon.*, *45*(2), 109–208. https://doi.org/10.1016/S0079-6611(99)00052-X

Hermanson, L., Eade, R., Robinson, N. H., Dunstone, N. J., Andrews, M. B., Knight, J. R., et al. (2014). Forecast cooling of the Atlantic subpolar gyre and associated impacts. *Geophysical Research Letters*, *41*, 5167–5174. https://doi.org/10.1002/2014GL060420

Holliday, N. P., Bersch, M., Berx, B., Chafik, L., Cunningham, S., Florindo-López, C., et al. (2020). Ocean circulation causes the largest freshening event for 120 years in eastern subpolar North Atlantic. *Nature Communications*, *11*(1), 585–515. https://doi.org/10.1038/s41467-020-14474-y

Houpert, L., Inall, M. E., Dumont, E., Gary, S., Johnson, C., Porter, M., et al. (2018). Structure and transport of the North Atlantic Current in the eastern subpolar gyre from sustained glider observations. *Journal of Geophysical Research: Oceans*, *123*, 6019–6038. https://doi.org/10.1029/2018JC014162

Kanzow, T., & Zenk, W. (2014). Structure and transport of the Iceland Scotland Overflow plume along the Reykjanes Ridge in the Iceland Basin. *Deep Sea Research Part I: Oceanographic Research Papers*, *86*, 82–93. https://doi.org/10.1016/J.DSR.2013.11.003

Knutsen, Ø., Svendsen, H., Østerhus, S., Rossby, T., & Hansen, B. (2005). Direct measurements of the mean flow and eddy kinetic energy structure of the upper ocean circulation in the NE Atlantic. *Geophysical Research Letters*, *32*, L14604. https://doi.org/10.1029/2005GL023615

Lebedev, K. V., Yoshinari, H., Maximenko, N. A., & Hacker, P. W. (2007). YoMaHa'07: Velocity data assessed from trajectories of Argo floats at parking level and at the sea surface. Retrieved from http://apdrc.soest.hawaii.edu/projects/yomaha/yomaha07/YoMaHa070612small.pdf

Lherminier, P., Mercier, H., Huck, T., Gourcuff, C., Perez, F. F., Morin, P., et al. (2010). The Atlantic Meridional Overturning Circulation and the subpolar gyre observed at the A25-OVIDE section in June 2002 and 2004. *Deep Sea Research Part I: Oceanographic Research Papers*, *57*(11), 1374–1391. https://doi.org/10.1016/J.DSR.2010.07.009

Mercier, H., Lherminier, P., Sarafanov, A., Gaillard, F., Daniault, N., Desbruyères, D., et al. (2015). Variability of the meridional overturning circulation at the Greenland–Portugal OVIDE section from 1993 to 2010. *Progress in Oceanography*, *132*, 250–261. https://doi.org/10.1016/J.POCEAN.2013.11.001

Petit, T., Mercier, H., & Thierry, V. (2018). First direct estimates of volume and water mass transports across the Reykjanes Ridge. *Journal of Geophysical Research: Oceans*, *123*, 6703–6719. https://doi.org/10.1029/2018JC013999

Petit, T., Mercier, H., & Thierry, V. (2019). New insight into the formation and evolution of the east Reykjanes Ridge Current and Irminger Current. *Journal of Geophysical Research: Oceans*, *124*, 9171–9189. https://doi.org/10.1029/2019JC015546

Read, J. F. (2000). CONVEX-91: Water masses and circulation of the Northeast Atlantic subpolar gyre. *Progress in Oceanography*, *48*(4), 461–510. https://doi.org/10.1016/S0079-6611(01)00011-8

Read, J. F., & Pollard, R. T. (2001). A long-lived eddy in the Iceland Basin 1998. *Journal of Geophysical Research, Oceans*, *106*(C6), 11,411–11,421. https://doi.org/10.1029/2000JC000492

Rio, M. H., Guinehut, S., & Larnicol, G. (2011). New CNES-CLS09 global mean dynamic topography computed from the combination of GRACE data, altimetry, and in situ measurements. *Journal of Geophysical Research*, *116*(C7), C07018. https://doi.org/10.1029/2010JC006505

Roemmich, D., & Gilson, J. (2009). The 2004–2008 mean and annual cycle of temperature, salinity, and steric height in the global ocean from the Argo Program. *Progress in Oceanography*, *82*(2), 81–100. https://doi.org/10.1016/J.POCEAN.2009.03.004

Sarafanov, A., Falina, A., Mercier, H., Sokov, A., Lherminier, P., Gourcuff, C., et al. (2012). Mean full-depth summer circulation and transports at the northern periphery of the Atlantic Ocean in the 2000s. *Journal of Geophysical Research*, *117*, C01014. https://doi.org/10.1029/2011JC007572

Saunders, P. M. (1996). The flux of dense cold overflow water southeast of Iceland. *Journal of Physical Oceanography*, *26*(1), 85–95. https://doi.org/10.1175/1520-0485(1996)026<0085:TFODCO>2.0.CO;2

Thierry, V., de Boisseson, E., & Mercier, H. (2008). Interannual variability of the Subpolar Mode Water properties over the Reykjanes Ridge during 1990–2006. *Journal of Geophysical Research, Oceans*, *113*, C04016. https://doi.org/10.1029/2007JC004443

Treguier, A. M., Theetten, S., Chassignet, E. P., Penduff, T., Smith, R., Talley, L., et al. (2005). The North Atlantic subpolar gyre in four high-resolution models. *Journal of Physical Oceanography* Retrieved from, *35*(5), 757–774. https://doi.org/10.1175/JPO2720.1

van Aken, H. M., & Becker, G. (1996). Hydrography and through-flow in the north-eastern North Atlantic Ocean: The NANSEN project. *Progress in Oceanography*, *38*(4), 297–346. https://doi.org/10.1016/S0079-6611(97)00005-0

van Aken, H. M., & de Boer, C. J. (1995). On the synoptic hydrography of intermediate and deep water masses in the Iceland Basin. *Deep Sea Research Part I: Oceanographic Research Papers*, *42*(2), 165–189. https://doi.org/10.1016/0967-0637(94)00042-Q

Wade, I. P., & Heywood, K. J. (2001). Tracking the PRIME eddy using satellite altimetry. *Deep Sea Research Part II: Topical Studies in Oceanography*, *48*(4–5), 725–737. https://doi.org/10.1016/S0967-0645(00)00094-1

Xu, X., Schmitz, W. J., Hurlburt, H. E., Hogan, P. J., & Chassignet, E. P. (2010). Transport of Nordic Seas overflow water into and within the Irminger Sea: An eddy-resolving simulation and observations. *Journal of Geophysical Research*, *115*, C12048. https://doi.org/10.1029/2010JC006351

Yashayaev, I. (2007). Hydrographic changes in the Labrador Sea, 1960–2005. *Progress in Oceanography*, *73*(3-4), 242–276. https://doi.org/10.1016/j.pocean.2007.04.015

Yashayaev, I., Bersch, M., & van Aken, H. M. (2007). Spreading of Labrador sea water to the Irminger and Iceland basins. *Geophysical Research Letters*, *34*, L10602. https://doi.org/10.1029/2006GL028999

Yashayaev, I., & Clarke, A. (2008). Evolution of North Atlantic water masses inferred from Labrador Sea salinity series. *Oceanography*, *21*(1), 30–45. https://www.jstor.org/stable/24860152?seq=1#metadata_info_tab_contents, https://doi.org/10.5670/oceanog.2008.65

Yashayaev, I., & Dickson, R. R. (2008). Transformation and fate of overflows in the northern North Atlantic. In R. R. Dickson, J. Meincke, P. Rhines (Eds.), *Arctic-subarctic ocean fluxes: Defining the role of the Northern Seas in climate* (pp. 505–526). New York: Springer.

Yashayaev, I., & Loder, J. W. (2016). Recurrent replenishment of Labrador sea water and associated decadal-scale variability. *Journal of Geophysical Research: Oceans*, *121*, 8095–8114. https://doi.org/10.1002/2016JC012046

Zhao, J., Bower, A., Yang, J., Lin, X., & Zhou, C. (2018). Structure and formation of anticyclonic eddies in the Iceland Basin. *Journal of Geophysical Research: Oceans*, *123*, 5341–5359. https://doi.org/10.1029/2018JC013886